Progress in Organic Coatings 174 (2023) 107269

Contents lists available at ScienceDirect

Progress in Organic Coatings

journal homepage: www.elsevier.com/locate/porgcoat

Copper-chitosan nanoparticles incorporated PGS/MAO bilayer coatings for potential cardiovascular application

Mohsen Ghafarzadeh, Mahshid Kharaziha *, Masoud Atapour, Parisa Heidari

Department of Materials Engineering, Isfahan University of Technology, Isfahan 84156-83111, Iran

ARTICLE INFO

Keywords:
Copper-chitosan nanoparticle
Blood compatibility
Nitric oxide release
Biodegradable AZ91 alloy

ABSTRACT

This study aims to develop bilayer copper-chitosan nanoparticles (Cu-Ch NPs) incorporated polyglycerol sebacate (PGS)/ micro-arc oxidation (MAO) (MAO-PGS/Cu-Ch NPs) coating for the cardiovascular application. Moreover, the effects of Cu-Ch NP concentrations (1, 3, and 5 wt%) on the physical, chemical, electrochemical, and biological properties of AZ91 substrate are discussed. Microstructural studies show the successful incorporation of Cu-Ch NPs in the PGS coatings using a simple electrospray process, improving surface wettability and roughness. The results of the potentiodynamic polarization test in phosphate buffer saline (PBS) indicate that the highest corrosion resistance (I_{corr} = 20 nA/cm^2, E_{corr} = −1.22 V) is obtained by adding 5 wt% Cu-Ch NPs. NO release evaluation shows while the burst release occurrs in the early hours, the extended-release happens after 12 h. Moreover, the increase in the Cu-Ch NP concentration reduces the platelet adhesion, showing the appropriate hemocompatibility of coatings. In addition, the attachment and proliferation of human umbilical vein endothelial cells (HUVECs) improve by increasing the concentration of Cu-Ch NPs within the bilayer coating. Taken together, MAO-PGS/Cu-Ch NPs coating with appropriate surface properties, corrosion resistance, cytocompatibility and hemocompatibility, demonstrates the potential application for cardiovascular implants.

1. Introduction

In recent decades, coronary artery disease has been the leading cause of mortality in cardiovascular disease [1]. To treat this disease, various cardiovascular implants have been developed. Between them, biodegradable materials such as magnesium alloys have been applied as temporary implants due to their biodegradable features in physiological environments, superior mechanical properties than polymeric ones, reduced thrombosis, and neointima hyperplasia. AZ91 alloy is of the most common magnesium-aluminum–zinc alloys used for biomedical applications. AZ91 is able to provide proper corrosion behavior and degradation rate via the formation of a passivating oxide layer. AZ91 has demonstrated biocompatibility and hemocompatibility in biological conditions. Moreover, it shows appropriate mechanical strength (240–250 MPa), elastic modulus (45 GPa), and elongation (3–7 %) for tissue engineering [2]. However, the most critical challenge of magnesium alloys is their rapid degradation rate associated with hydrogen evolution, the release of high concentrations of magnesium ions, and the local increase in pH, which may adversely affect the patient's health [3]. Numerous surface modifications and coating strategies have been used to improve the corrosion behavior of magnesium-based implants in a physiological environment. Between them, micro-arc oxidation (MAO) is one of the reliable methods to develop satisfied adhesion with appropriate corrosion behavior and wear resistance [4]. However, some limitations of MAO coatings, such as large pore size, may affect the long-term function of implants [5].

Various polymeric and nanocomposite coatings have been developed to fill the porosity of MAO coatings leading to improved corrosion resistance, biocompatibility, and degradation rate [6]. While both synthetic and natural polymers have been used as coatings for biomedical applications [7], synthetic polymers are more promising due to their flexibility and controlled degradation rate [8]. Recently, we have developed poly (glycerol sebacate) (PGS) coating on MAO-coated AZ91 substrate and found the improvement of the surface properties and corrosion resistance of the substrate by applying a bilayer MAO/PGS coating [9]. PGS has been the subject of numerous studies for cardiovascular tissue engineering, due to its biocompatibility, biodegradability, mechanically compatibility, and low immunogenic impacts [10]. Despite the advantages of PGS coatings, accelerating vascular regeneration and angiogenesis without using growth factors and drugs

* Corresponding author.
E-mail address: kharaziha@cc.iut.ac.ir (M. Kharaziha).

https://doi.org/10.1016/j.porgcoat.2022.107269
Received 26 August 2022; Received in revised form 9 October 2022; Accepted 11 October 2022

to stimulate endothelial cell proliferation and to prevent the growth of smooth muscle cells (SMCs) and blood clotting is not possible [11]. Various drugs and growth factors have been applied to accelerate endothelial cell proliferation, including deferoxamine [12], vaccarin [13], asperosaponin VI [14], and nitric oxide [15]. Between them, nitric oxide (NO) acts as a signaling molecule to increase angiogenesis and NO release has been introduced as a novel and successful approach for cardiovascular applications. NO prevents hyperplasia in blood vessels and controls the growth and proliferation of SMCs without causing cytotoxicity [16]. In addition, NO prevents platelet adhesion and thrombosis and plays an essential role in regulating vascular homeostasis [16]. Recently, a novel NO generator based on the copper-chitosan system has developed by Fontana et al. [15]. In this system, nitrite was reduced by oxidation of the copper (Cu^{+1}) to Cu^{+2} state, and NO was generated. Furthermore, copper ions were mainly engaged in angiogenesis, vasculogenesis, and endothelial cell migration as a stimulus. In addition, it has been demonstrated that, Cu^{+2} enhanced the growth and angiogenesis-related gene expression of HUVECs [17].

This study aims to develop a bilayer copper-chitosan nanoparticles (Cu-Ch NPs) incorporated PGS-MAO (MAO-PGS/Cu-Ch NPs) coating to improve endothelial cell proliferation and blood compatibility of magnesium alloy. Furthermore, the role of bilayer MAO-PGS/Cu-Ch NPs coating on corrosion behavior and biological properties of AZ91 alloy is investigated. Following the MAO coating, PGS/Cu-Ch NPs layer is developed on MAO porous layer using the electrospray method. Moreover, the role of Cu-Ch NP concentration (0, 1, 3 and 5 wt%) on the corrosion behavior, hemocompatibility and biological properties of AZ91 is investigated. It is hypothesized that while Cu-Ch NPs stimulate NO generation, both PGS and Cu-Ch NPs improve the corrosion resistance and hemocompatibility of AZ91 alloy.

2. Material and methods

2.1. Materials

AZ91 alloy (National Metallurgical Laboratory, India) with the composition of 8.63 wt% aluminum, 0.59 wt% zinc, 0.17 wt% manganese, <0.05 wt% copper, <0.05 wt% of iron, and the balanced magnesium was used. Samples with dimensions of 10 × 10 × 3 mm^3 were prepared from AZ91 ingots using wire-cut, and then their surface was polished using 80, 120, 600, 800, 1200, and 2000 sandpaper. To eliminate contamination from the surface of the substrates, they were rinsed with ethanol in an ultrasonic bath for 20 min. Finally, they were dried at room temperature. PGS polymer was also synthesized according to our previous study [9]. To prepare composite coatings, acetone (99.0 %), ethanol (99.0 %), sodium silicate (99.9 %), sodium hydroxide (99.9 %), sodium fluoride (99.9 %) was supplied from Merck co. To synthesize Cu-Ch NPs, chitosan (degree of deacetylation = 85 %, Sigma), $CuSO_4.5H_2O$ (Merck, 99.0 %), acetic acid (Merck, 100 %), ascorbic acid (Sigma, 99.0 %) and hydrazine hydrate (Merck, 99.0 %) were provided.

2.2. Synthesis of copper-chitosan nanoparticles (Cu-Ch NPs)

Cu-Ch NPs were in situ-synthesized using the chemical method, according to our previous study [18]. Briefly, 0.05 M acetic acid solution (80 ml) containing 4 g/l chitosan was mixed with 20 ml of 0.07 M copper sulfate solution for 90 min. Then, 1 ml of 0.5 M ascorbic acid and 4 ml of 0.6 M sodium hydroxide were added to provide a green solution. After 90 min, 1 ml of hydrazine was added to the solution to turn it into red color. After 24 h mixing at room temperature, the resulting copper-chitosan nanoparticles were filtered and air-dried.

2.3. Development of bilayer MAO-PGS/Cu-Ch NPs coating

The MAO layer was first created on the substrate to develop a bilayer nanocomposite coating, similar to our previous study [9]. MAO process was performed in an electrolyte solution containing sodium silicate(100 g/l), sodium hydroxy (100 g/l), and sodium fluoride (20 g/l) at a constant voltage of 60 V and a working distance of 2 cm for 45 min. To develop the second PGS/Cu-Ch NPs layer, 10 wt% PGS solution in acetone: ethanol solution with a volume ratio of 3:7 was used. At this stage, different concentrations of Cu-Ch NPs (0, 1, 3, and 5 wt%) were added to the PGS solution, mixed for 4 h at room temperature and ultrasonicated for 1 h before the coating process.

Electrospray of the PGS/Cu-Ch NPs layer was performed using a 23G blunted stainless steel needle. Electrospray parameters were set as follows: feed rate = 0.5 ml/h, coating time = 7 h, voltage = 17 kV, and working distance = 15 cm. After the coating process, the samples were crosslinked at 125 °C for 4 h under a vacuum of 0.015 mmHg. According to the concentration of Cu-Ch NPs (0, 1, 3 and 5 wt%), the samples were named Cu-Ch-0 %, Cu-Ch-1 %, Cu-Ch-3 % and Cu-Ch-5 %, respectively.

2.4. Physicochemical characterization of bilayer MAO-PGS/Cu-Ch NPs coating

To investigate the particle size distribution of Cu-Ch NPs and their surface charge, the dynamic light scattering (DLS) method and zeta potential were performed using Particles size and Zeta potential Analyzer (SZ-100-Horiba). The morphology of nanoparticles and bilayer coatings were studied using scanning electron microscopy (SEM, S360) after gold-sputter coating. The average surface porosity of the bilayer coatings was also estimated using ImageJ software. X-ray diffractometer (XRD, Philips X'Pert) using CuKα radiation was used for chemical characterization of Cu-Ch NPs and MAO-PGS/Cu-Ch NPs coatings. To investigate the functional groups in Cu-Ch NPs and bilayer coatings, Fourier transform infrared (FTIR) spectroscopy was performed in the range of 600–4000 cm^{-1} and the resolution was set to 2 cm^{-1}. The coatings thickness (n = 3) was measured by the coating thickness gauge (Sonowall 70), and the average thickness value was reported from three points. To investigate the surface roughness of the sample, the roughness tester (Taylor-Hobson Surtronic Duo) was used, and the average value of roughness (Ra) and the surface profile were provided. Furthermore, the water contact angle of the samples was evaluated using a contact angle measuring device (Jikan CAG-20, Iran). 4 μl of water drop fell on samples (n = 3), and the water contact angle was estimated after 4 s.

The international standard ISO 13779-4 was used to study the adhesion strength of coatings. The coated samples with a dimension of 10 × 10 mm were attached to the two steel jaws with 10 mm diameter using glue (Uhu Epoxy ultra-strong, Germany) and kept for 24 h at room temperature. Then, a tensile test was designed with a rate of 0.2 mm/min and the force-expansion graph was plotted. Finally, the average adhesion strength of three samples was reported. In addition, the release of Cu ions from samples after 5 days of soaking in phosphate buffer solution (PBS, pH = 7.4) was assessed using an inductively coupled plasma mass spectrometry (ICP) assay (Optima 7300 V ICP-OES HF, PerkinElmer, USA).

2.5. Electrochemical corrosion evaluation of bilayer MAO-PGS/Cu-Ch NPs coating

The corrosion resistance of MAO-PGS/Cu-Ch NPs coated samples was evaluated using the potentiodynamic polarization test. The corrosion resistance was studied in PBS at 37 ± 1 °C using AMETEK potentiostat/galvanostat (PARSTAT 2273). This test was performed using a conventional three-electrode cell setup, including a reference Ag/AgCl (saturated in KCl), the counter platinum, and the working (the sample) electrodes. Before the corrosion test, the coated samples were immersed in PBS for 1 h to reach a constant open-circuit potential value. The potential scan range was considered −250 – +250 mV vs. the open circuit potential, and the scan rate was set 1 mV/s. According to ASTM-G102–89 standard E_b (Breakdown Potential), E_{corr}, I_{corr}, βa, βc, and R_p were obtained by the polarization diagram extrapolation. SEM imaging

was also used to investigate the corroded surfaces.

2.6. Nitric oxide release from bilayer MAO-PGS/Cu-Ch NPs coating

To evaluate the role of Cu-Ch NPs on the NO release, the NatrixTM Nitric Oxide (NO) assay kit (Navand Salamat Co., Iran) was used. NO release from bilayer MAO-PGS/Cu-Ch NPs coating was detected by the Griess Reagent method, according to the manufacturer's protocol. Briefly, the samples were weighted and soaked in PBS with the ratio of 1 g of sample: 100 ml of PBS for 24 h and at room temperature. To evaluate the NO release from the soaked samples, 150 µl of each PBS solution was poured into 2 ml-microtubes, and consequently, 80 µl of nitrate was added to the microtubes and vortexed for 30 s. Then, 80 µl of nitrate reductase was added to the microtubes, and the microtubes were placed in a centrifuge at 14,000 rpm for 10 min to remove particles and impurities. Following the addition of 50 µl of solutions to the 96-well plate, 50 µl of Griess Reagent I (R1) was added to the well-plate and incubated for 10 min, and, finally, 50 µl of Griess Reagent II (R2) was added to it and incubated for next 20 min. After mixing the reagents (50 µl of R1 + 50 µl of R2 + 50 µl of the sample), the optical density (OD) value was recorded using a microplate reader at 540 nm. In this study, the Cu-Ch-0 % sample was considered a control sample to prevent polymer interference in NO absorption (due to polymer degradation) and Griess reagent reaction. The produced NO was estimated by calculating the difference in adsorption between Cu-Ch-5 % and Cu-Ch-0 %.

2.7. Protein adsorption study

The ability of the samples to adsorb protein molecules was studied using bovine serum albumin (BSA), according to previous studies [19]. Following the soaking in PBS, the samples were weighed (W), washed twice with PBS and soaked in BSA solution (50 µg/ml) for 30 min. The BSA concentration was selected according to recent studies [20]. Finally, UV–vis spectroscopy (UNICO, S2150, USA) was applied at 280 nm and the adsorbed protein (µg /g) was estimated according to Eq. (1) [19]

$$\text{Adsorbed BSA} = \left(\frac{\mu g}{g}\right) = \frac{C_0 - C_a}{w} \times V \quad (1)$$

where V was the original volume of BSA solution, and C_0 and C_a were the BSA concentration before and after adsorption on the coatings, respectively. The BSA concentration before and after adsorption was estimated according to the standard curve of BSA provided in the concentration range of 0.02–4 (mg/ml) at 280 nm.

2.8. Cell culture

Cytocompatibility of samples was investigated using the culture of human umbilical vein endothelial cells (HUVECs, Royan Institute, Iran) in direct contact with samples. Before cell culture, samples were immersed in 70 % ethanol for 20 min and exposed to ultraviolet light (UVC, wavelength: 200–280 nm) for 20 min. Then, the cells were seeded on samples, and tissue culture plate (TCP, control) with a density of 10^4 cells/well and incubated in Dulbecco's Modified Eagle Medium (DMEM, Bioidea) supplemented with 10 % Feral bovine serum (FBS, Sigma) and 1% penicillin/streptomycin (Pen/Strep, Bioidea) at 37 °C for 5 days. To examine the cell attachement and spreading on samples, after removing the culture medium, the cell-seeded samples were immersed in 2.5 % glutaraldehyde (Sigma) for 20 min and then dehydrated by gradient ethanol solutions (30 %, 70 %, 90 %, 96 %, and 100 % ethanol, respectively). The samples were kept in a desiccator until imaging. Finally, the cell morphology was examined using SEM imaging.

3-(4,5-Dimethylthiazol-2-yl)-2,5 Diphenyltetrazoliumbromid) (MTT) assay was performed according to the manufacturers' protocol (Sigma) to evaluate the cytocompatibility of bilayer coatings. At specified time points (1, 3, and 5 days), the medium was slowly removed from the cell-seeded samples and replaced with MTT solution (0.5 mg/ml) (n = 3). After 3 h incubation at 37 °C under 5 % CO_2, dimethyl sulfoxide (DMSO, Sigma) was added to the culture medium to dissolve the formazan crystals. Finally, the absorption of the solution was measured by an ELISA microplate reader at a wavelength of 490 nm, and the cell viability was calculated based on Eq. (2) [21]:

$$\text{Relative cell survival (\%control)} = \frac{A_{sample} - A_{blank}}{A_{control} - A_{blank}} \times 100 \quad (2)$$

where A_{sample} was the absorbance of samples and $A_{control}$ and A_{blank} were the absorbance of the control (TCP) and blank (DMSO), respectively.

2.9. Platelet adhesion

Platelet adhesion on the samples was investigated, according to a previous study [22]. In this regard, the blood of a volunteer adult containing 10 % sodium citrate anticoagulant was provided. It needs to mention that sodium citrate could stabilize blood and blood products, by presumably sequestering Ca^{2+} ions in vitro [23]. 30 ml of human blood was centrifuged at 6000 rpm for 30 min to separate plasma-rich platelet (PRP) from red and white cells. Then, the samples were incubated with PRP at 37 °C for 2 h. The samples were washed three times with PBS and subsequently immersed in 2.5 % glutaraldehyde at room temperature for 45 min. After rinising with PBS, the samples were air-dried and finally, the platelet adhesion was examined by SEM imaging.

2.10. Statistical analysis

The statistical significance difference between the results in various groups of samples was determined using one-way ANOVA ($n \geq 3$) and Tukey's post-hoc test. P-value<0.05 was determined to be significant.

3. Result and discussion

3.1. Characterization of Cu-Ch NPs

Cu-Ch NPs were in-situ synthesized using a simple and one-step process, according to Fig. 1A. XRD pattern of Cu-Ch NPs (Fig. 1B) consisted of two peaks at $2\theta = 20°$ and 23° originating from the chitosan structure [24]. In addition, peaks related to pure copper were found at $2\theta = 43°$, 50°, and 74°, originating from (111), (200), and (220) in the face centered cubic (FCC) structure of copper, respectively. Copper oxide peaks (CuO) at $2\theta = 32°$, 35°, 38°, and 48° also corresponded to (110), (002), (111), and (202) of the monoclinic structure, respectively [25]. The Cu/CuO ratio calculated according to Automated Reference Intensity Ratio Analysis [26], was estimated about 0.45. In addition, the FTIR spectrum of Cu-Ch NPs, compared to chitosan (Fig. 1C) confirmed the presence of chitosan in the nanoparticles. The spectrum of chitosan consisted of a broad peak at 3349 cm^{-1} corresponded to the N—H stretching bond and the O—H hydrogen bond. Moreover, two peaks at 2880 cm^{-1} and 2920 cm^{-1} were related to the C—H vibrating of chitosan. The characteristic peaks of the CH_2 group and the amide bond C—N (type III) were also identified at 1420 cm^{-1} and 1320 cm^{-1}, respectively. In addition, the peaks located at 1590 cm^{-1}, 1650 cm^{-1}, and 1165 cm^{-1} corresponding to the N—H vibration bond (type II) and C—O stretching bond, respectively. Finally, the peaks at 1150 cm^{-1} and 896 cm^{-1} were related to the C—O—C stretching bond and the saccharide structure of chitosan monomers [27]. In the spectrum of Cu-Ch NPs, the change in the shape and intensity of bending and stretching bonds of C—H at 1420 cm^{-1}, 2880 cm^{-1}, and 2920 cm^{-1} was revealed, which might be due to the changes in the CH_2OH group, originating from the reaction between the amine groups in complexing with Cu particles. In addition, the chitosan characteristic peak at 3349 cm^{-1} was shifted to 3370 cm^{-1} after forming Cu-Ch NPs. The same peak shifting

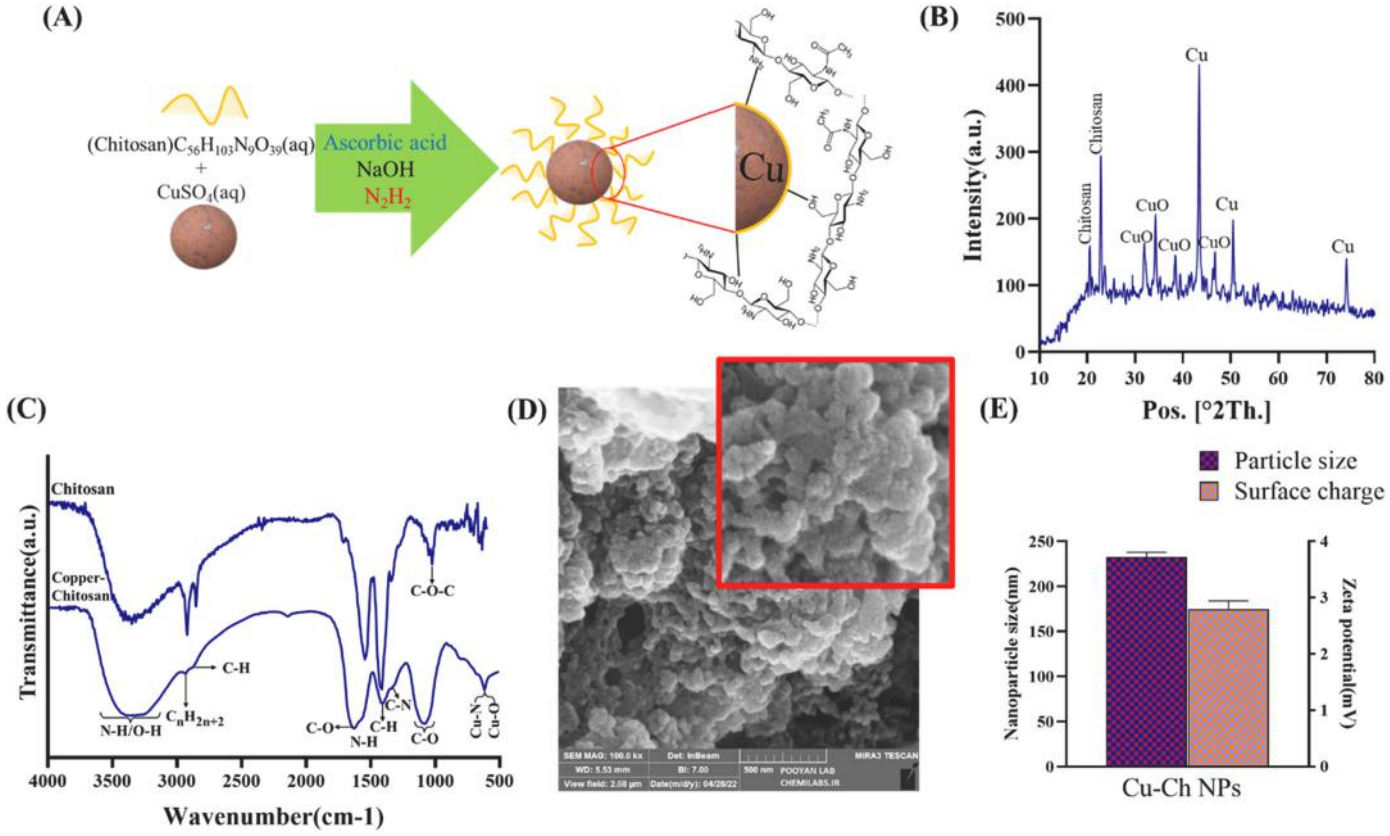

Fig. 1. Physicochemical properties of Cu-Ch NPs: (A) Schematic of the synthesis of Cu-Ch NPs. (B) XRD pattern of Cu-Ch NPs. (C) FTIR spectra of chitosan and Cu-Ch NPs. (D) SEM image of Cu-Ch NPs. (E) Particle size and Zeta potential of Cu-Ch NPs.

was reported in previous research [24]. Moreover, the peak at 1650 cm^{-1} also belonged to the first type of amide group, which was attributed to the C—O stretching and N—H deformation mode in the glucosamine unit(—$CONH_2$). In addition, the peak at 620 cm^{-1} was related to Cu—N and Cu—O bonds confirming to the formation of chemical bonds between copper ions and chitosan structure (NH^+ and OH^-) [18,21].

Morphology of Cu-Ch NPs was also examined by SEM. According to Fig. 1D, Cu-Ch nanopowder with uniform particles in an approximately spherical shape was developed. There was an aggregation of nanoparticles in the distribution. It might be due to the high surface energy of nanoparticles which was associated with their small size and low concentration of chitosan [28]. Usman et al. [28] also reported high agglomeration of the copper-chitosan complex at low chitosan concentrations. In addition, according to the DLS and zeta potential results (Fig. 1E), the Cu-Ch NPs with an average size of 218 ± 19 nm were synthesized. The results were consistent with the research of Usman et al. [28], who synthesized copper NPs in the size range of 2–300 nm using a chemical reaction method. In addition, the surface charge of Cu-Ch NPs was determined to be 2.7 ± 0.2 mV, originating from the positive surface charge of chitosan covering the nanoparticles. As reported in other studies, the positive surface charge of Cu-Ch NPs could provide electrostatic interaction with PGS with a negatively charged surface [29].

3.2. Physicochemical properties of bilayer MAO-PGS/Cu-Ch NPs coatings

In the next step, bilayer MAO-PGS/Cu-Ch NPs were developed using a two-step MAO and electrospray process (Fig. 2A). According to the SEM images (Fig. 2B), the incorporation of Cu-Ch NPs changed the porosity, and uniformity of coatings, depending on the NP content (Fig. 2C). While the MAO-PGS coating (Cu-Ch-0 %) revealed a uniform morphology, incorporation of Cu-Ch NPs reduced the surface uniformity and protrusions were formed specifically when 3 and 5 wt% Cu-Ch NPs were incorporated. In addition, the average pore size of the coating increased from 10.7 ± 4.1 μm to 13.4 ± 4 μm after the incorporation of 5 wt% Cu-Ch NPs. The distribution of Cu-Ch NPs in the layer was also investigated using copper EDS mapping (Fig. 2D). While the agglomeration of the copper element in the surface of Cu-Ch-3 % and Cu-Ch-5 % coatings was observed, uniform distribution of nanoparticles was detected on the Cu-Ch-1 % sample. Saraswathi et al. [30] also found that the incorporation of different concentrations of polyhexanide-coated CuO NPs into the polyvinylidene fluoride (PVDF) could increase the pore size and porosity of neat PVDF due to the agglomeration of nanoparticles. Based on previous studies, the pore size of coatings in the range of 10–40 μm could be acceptable for cardiovascular applications. Cells can penetrate holes and attach to porous structures with pore sizes ranging from 10 to 40 μm. As a result of the cell adhesion to the porous structure, cell growth and proliferation occur [31]. Our result also demonstrated that the incorporation of Cu-Ch NPs did not significantly change the thickness of coatings. Based on Fig. 2C, the thickness of coatings was in the range of 124–135 μm. According to previous studies, this thickness could be acceptable to promote corrosion resistance [32].

XRD patterns of bilayer coatings also demonstrated the presence of Cu-Ch NPs (Fig. 2E). Compared to the XRD pattern of MAO-PGS (Cu-Ch-0 %), the incorporation of 5 % Cu-Ch NPs (Cu-Ch-5 %) resulted in the formation of new peaks related to Cu-Ch NPs at $2\theta = 23°$, 35° and 43°. In addition, other peaks related to MAO at $2\theta = 42°$ ($MgSiO_3$, MgO), 52° (Mg_2SiO_4), 63° (MgO, MgF_2), and 79°(MgO) were also identified. Moreover, the peaks at $2\theta = 19°$ and 24° were related to the PGS coating. FTIR spectrum of Cu-Ch-5 %, compared to that of Cu-Ch-0 % is provided in Fig. 2F. Results showed that in addition to the characteristic peaks related to MAO-PGS, some new peaks appeared, and some peaks had intensity changes. For instance, a new peak at 629 cm^{-1} was detected

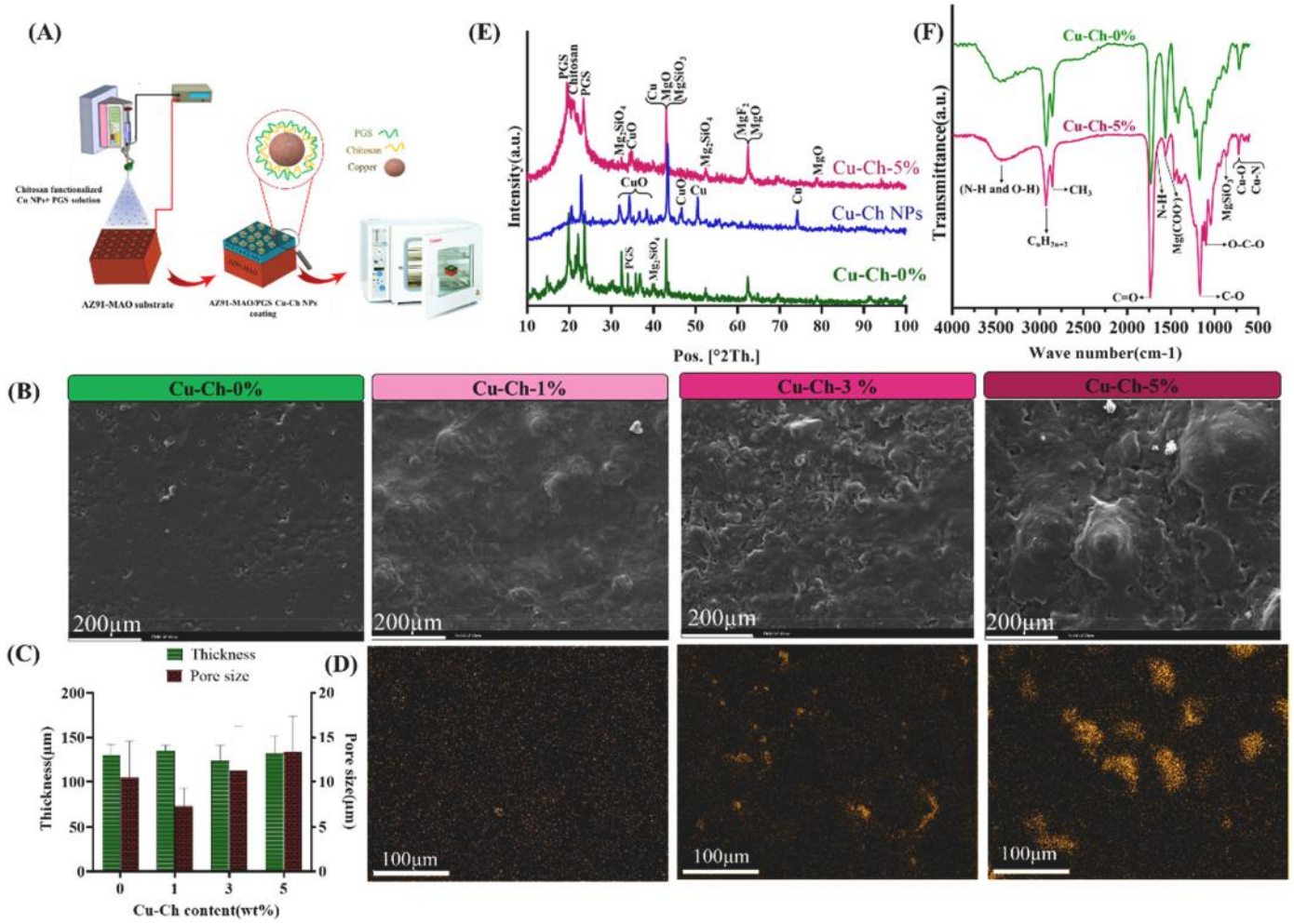

Fig. 2. Physicochemical properties of bilayer MAO-PGS/Cu-Ch NPs coatings: (A) Schematic of the formation of the bilayer coating on AZ91 substrate. (B) SEM images, (C) the thickness and pore size, and (D) elemental mapping of bilayer coated samples. (E) XRD patterns of Cu-Ch NPs, Cu-Ch-0 %, and Cu-Ch-5 %. (F) FTIR spectra of Cu-Ch-0 % and Cu-Ch-5 % samples.

due to Cu—O and Cu—N bonds. The intensity of the O—C—O vibrational bond at 1097 cm^{-1} increased due to the incorporation of chitosan in the PGS coating. The sharp peak at 1160 cm^{-1} related to the C—O bond was also observed in both samples. In addition, both samples showed a peak at 1566 cm^{-1}, which was due to the formation of the metallic carboxylic bond. Furthermore, the incorporation of Cu-Ch NPs reduced the intensity of this peak. For the Cu-Ch-5 % sample, the intensity of peaks corresponding to the hydroxyl group and amide II group of chitosan was significantly reduced due to PGS grafting [33]. In addition, the N—H bond and the O—H hydrogen bond (3200–3700 cm^{-1}) were presented more widely and distributed with lower intensity in the Cu-Ch-5 % sample, which might be due to the combination of the PGS matrix with chitosan. [33].

The role of Cu-Ch NPs on the surface roughness of bilayer coating was investigated. According to Fig. 3A, the surface profile of samples significantly changed with increasing Cu-Ch NP content. In addition, according to Fig. 3B, the average roughness of bilayer coatings greatly enhanced from 2.1 ± 0.1 µm (in Cu-Ch-0 %) to 6.7 ± 0.2 µm (in Cu-Ch-5 %) ($P < 0.05$). Similar result was reported for other nanocomposite coatings of chitosan/bioglass [34]. Surface roughness substantially affects the wettability, protein adsorption, platelet, and cell adhesion [34–36]. According to recent studies, with an increase in roughness, wettability increases as well [37], and also the surface roughness in the range of 0.1–13 µm could be suitable for EC proliferation and migration [36,38].

Moreover, the role of Cu-Ch NPs on the wettability of coating was investigated. According to Fig. 3C, the water contact angle of the samples significantly reduced from 36.7 ± 1.8° to <18.2 ± 0.9° after the incorporation of 5 wt% Cu-Ch NPs ($P < 0.05$). Various parameters could affect the surface wettability of coatings, including surface chemistry and roughness. As reported in previous studies, a significant increase in the roughness with increasing Cu-Ch NPs might result in a decrease in the water contact [37]. In addition, it should be noted that the intrinsic hydrophilicity of PGS and chitosan polymers could significantly influence the coating wettability [9,39]. Fadaie et al. [40] also demonstrated that incorporating 10 % chitosan into the polycaprolactone nanofibers reduced the water contact angle from 124° to 84°. Our results showed that Cu-Ch NPs significantly improved water contact angle, making it appropriate for biomedical applications [37,41]. High wettability provides more interaction between the environment and biomedical implants, which impacts corrosion behavior and biological activity [42].

The adhesive strength of the coating also plays an essential role in the mechanical property of the implant [43]. The role of Cu-Ch NPs on the adhesion strength of bilayer coatings was investigated, and the results are presented in Fig. 3D. The adhesion strength of coatings did not significantly change after the incorporation of 5 wt% Cu-Ch NPs. It might be due to the inefficacy of improved surface roughness of samples for enhancing adhesion strength [44]. This result was also reported in previous studies [44,45]. In some cases, reduced adhesion strength was also reported. For instance, according to Necati et al. [46] research, the

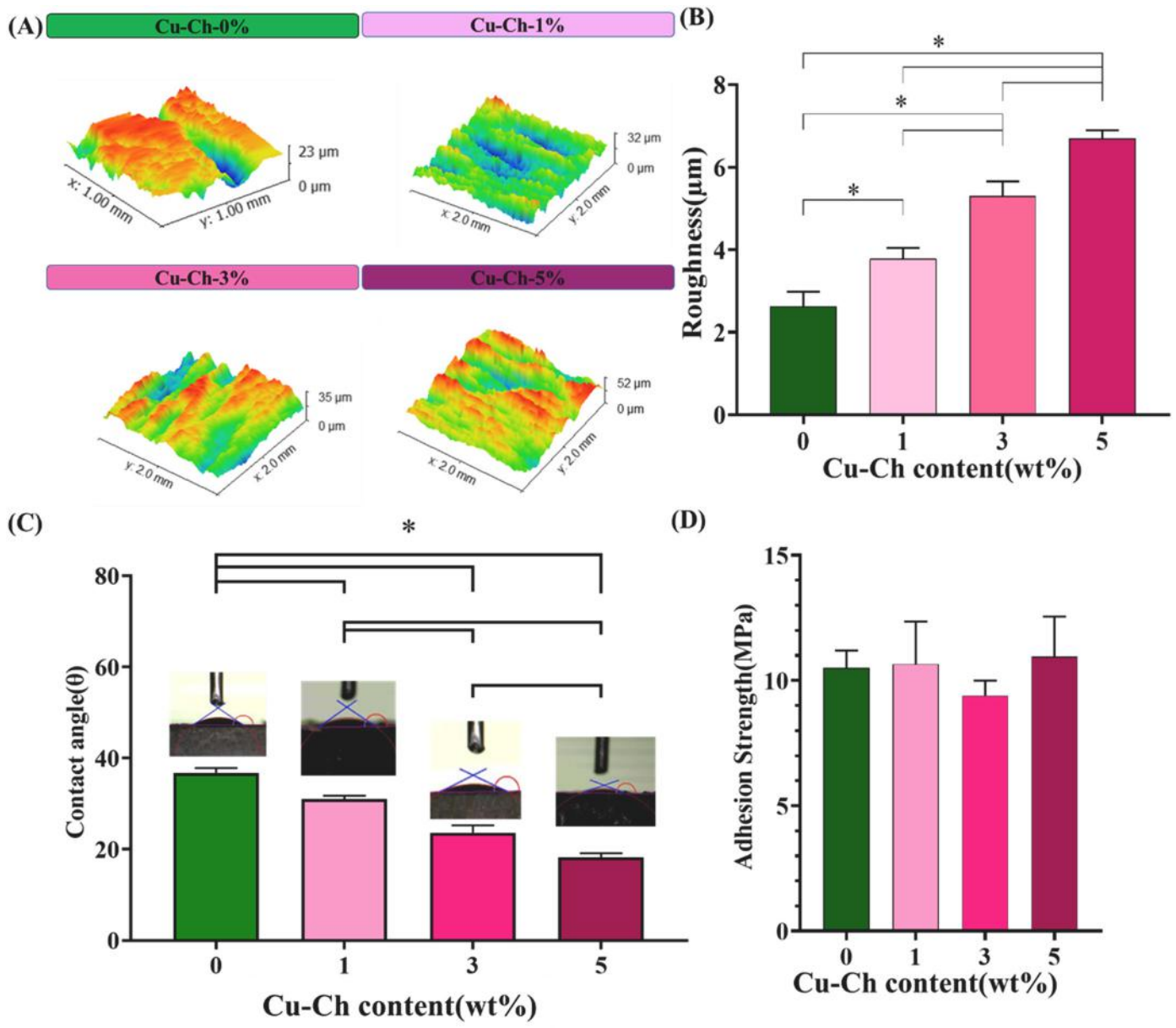

Fig. 3. Surface features of bilayer MAO-PGS/Cu-Ch NPs coatings: (A) 3D surface profile, (B) average surface roughness, (C) optical microscopic images of water contact angle and average water contact angle, as well as (D) the adhesion strength of bilayer coatings (*: significant difference, *P < 0.05, n = 3).

adhesion strength of epoxy resin coating decreased significantly after the incorporation of 5 wt% Cu NPs. In another study, Penin et al. [47] found the weakening of mechanical properties of polyester-ether-ketone after incorporation of 0.3 wt%Cu NPs. However, the PGS/Cu-Ch NPs nanocomposite coatings maintained mechanical stability and good adhesion strength.

3.3. Corrosion resistance of MAO-PGS/Cu-Ch NPs coated samples

The potentiodynamic polarization curves of MAO-PGS coatings consisting of various concentrations of Cu-Ch NPs (0, 1, 3, and 5 wt%) in PBS at 37 °C are presented in Fig. 4A. The parameters of corrosion current density, corrosion potential and breakdown potential were extracted from the anodic and cathodic curves of the diagrams and are presented in Fig. 4B. According to the results, the bilayer coatings induced a slight decrease in the current density in the anodic branch. In addition, nanocomposite layers provided a significant shift of the corrosion potential to the anodic direction. After incorporating 5 % Cu-Ch NPs into MAO/PGS coating, the E_{corr} of the Cu-Ch-0 % sample significantly increased from −1.47 V to −1.22 V. This corrosion behavior was attributed to the copper's nobility and the presence of chitosan as a cathodic corrosion inhibitor [48,49]. Kozina et al. [50] also found that chitosan coating on Mg-Zn alloy resulted in the reduced corrosion current density in Hank solution from 12.25 mA/cm^2 to 1 mA/cm^2 and increased corrosion potential from −1.47 V to −1.37 V. In our study, the presence of Cu-Ch NPs had a significant influence on the kinetics of anodic reactions. In the anodic region of the curves, a breakdown was observed, especially in the Cu-Ch-0 % and Cu-Ch-1 % samples. This effect might be attributed to the role of chloride in the dissolution. The chloride ions attacked on the passive layer and destroyed it which accelerated the corrosion process. As the consequences, some cracks appeared in the layers which provided new paths for electrolyte invasion [51]. The analysis of the E_b values revealed that the Cu-Ch-0 % and Cu-Ch-1 % samples illustrated the breakdown of coatings in $E_b = -1.26$ V and $E_b = -1.22$ V, respectively. Remarkably, no such breakdown was observed for Cu-Ch-3 % and Cu-Ch-5 % in the

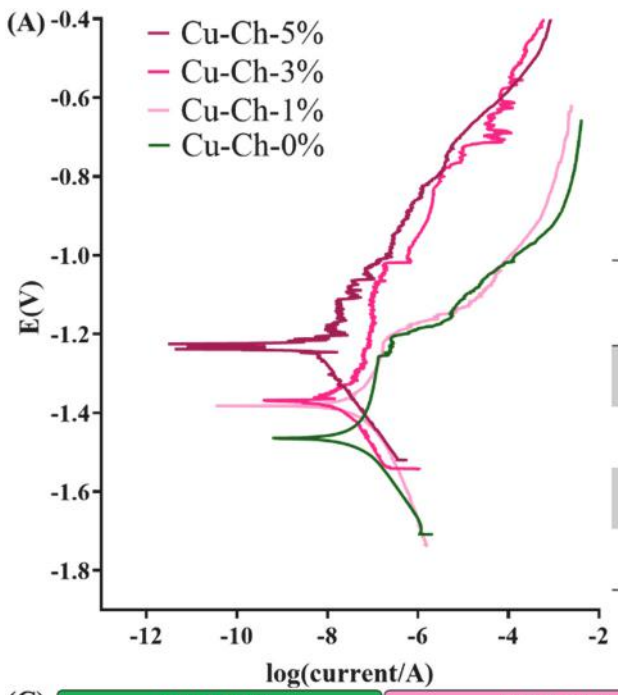

(B)

Samples	I_{corr} (μA/cm²)	E_{corr} (V)	E_b (V)	β_a(V/dec)	β_c(V/dec)	R_p(kΩ/cm²)
Cu-Ch-0%	0.04±0.02	-1.47±0.02	-1.26	0.1	0.163	1315±100
Cu-Ch-1%	0.03±0.01	-1.38±0.04	-1.22	0.125	0.246	1457±185
Cu-Ch-3%	0.028±0.01	-1.34±0.05	-	0.196	0.168	1745±136
Cu-Ch-5%	0.02±0.01	-1.22±0.02	-	0.154	0.153	1915±167

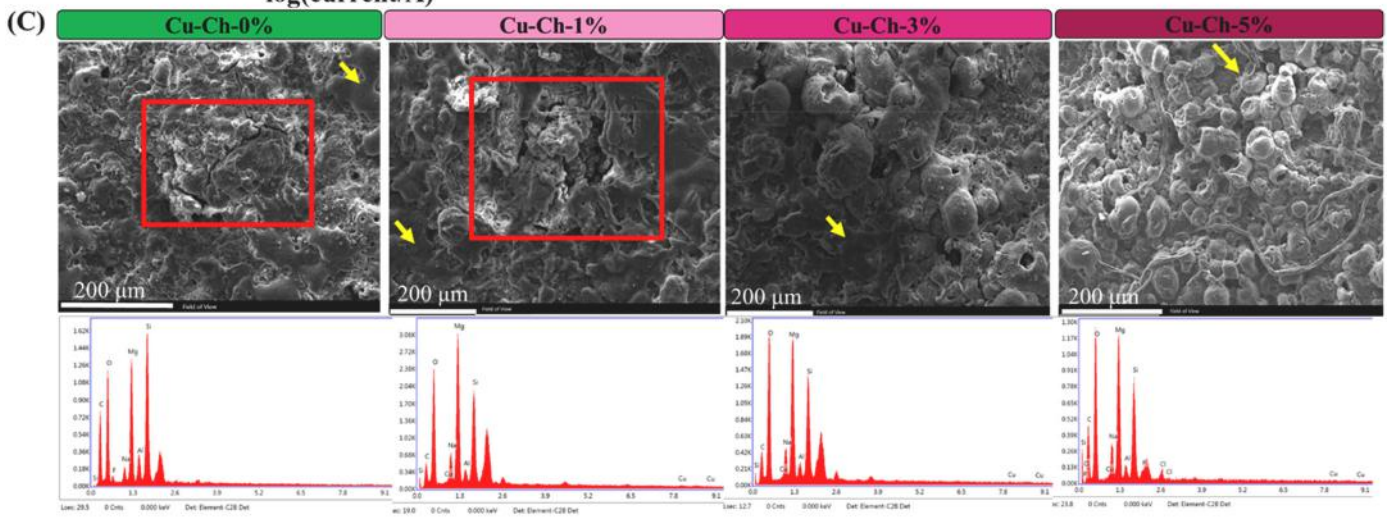

Fig. 4. (A) The potentiodynamic polarization curves of the MAO-PGS/Cu-Ch NPs coated samples immersed in PBS. (B) The potentiodynamic polarization parameters of all samples obtained after testing in PBS. (C) SEM-EDS analysis of the coated samples after potentiodynamic polarization test.

studied potential region. The formation of MAO/PGS-Cu-Ch NPs on AZ91 isolated the substrate from direct contact with PBS. This could imply an improvement in the local corrosion resistance of the samples by incorporating a higher concentration of Cu-Ch NPs in the PGS matrix, as similarly reported in other studies [48]. Notably, incorporation of Cu-Ch NPs in PGS coating resulted in slightly enhanced corrosion resistance (lower anodic current density). Fig. 4B shows that after the incorporation of 5 % Cu-Ch NPs (Cu-Ch-5 %) in the MAO/PGS coating (Cu-Ch-0 %), the corrosion current density reduced from 40 nA/cm^2 to 20 nA/cm^2. It might be due to the inhibitory effect and appropriate adhesion properties of both PGS and chitosan [49]. In similar research, Alaei et al. [34] significantly increased the corrosion resistance of AZ91 by applying chitosan coating containing different concentrations of Bio-glass nanoparticles. In this study, chitosan-0.5 % Bio-glass nanocomposite coating on AZ91 reduced the corrosion current density from 40 μA/cm^2 to 2 μA/cm^2.

The surface morphology of the bilayer coatings after the potentiodynamic polarization test is presented in Fig. 4C. Results showed the cracking corrosion mechanism in the corroded Cu-Ch-0 % and Cu-Ch-1 % (red square). These cracks could be the result of coating breakdown. However, Cu-Ch-3 % and Cu-Ch-5 % did not have these cracks which might be attributed to the improvement in corrosion behavior brought by increasing the concentration of Cu-Ch NPs. Microstructure and composition are the most crucial factors that determine corrosion behavior. In addition, other factors like roughness, wettability, and porosity also contribute to enhancing corrosion behavior [4]. The elemental analysis of the corroded samples is illustrated in Fig. 4C. The main elements, such as C, Na, Si, Mg, F, and O, were found in the analysis due to the presence of MAO and PGS bilayer. Moreover, copper was also found, which could be due to the residual polymer (yellow arrow) on the surface following the potentiodynamic polarization test. The percentage of elements such as oxygen, magnesium, and aluminum decreased with increasing nanoparticle concentration, which might be due to the enhanced corrosion resistance. According to the corroded surface images (Fig. 4C), by increasing the Cu-Ch NPs content, the cracks were significantly reduced in the MAO/PGS coating, confirming the enhanced corrosion resistance.

3.4. Nitric oxide release

Nitric oxide (NO) is a signaling molecule influential in infection, inflammation, and wound healing processes. NO has a meaningful role in physiological and angiogenic processes [15]. In this research, a new NO release system based on Cu-Ch NPs was developed. The samples were incubated in PBS to measure the release of NO in contact with the Cu-Ch-5 % sample. The representative NO release profile of Cu-Ch-5 % is shown in Fig. 5A. Following initial incubation, a burst release of NO was observed, followed by an extended NO release. The concentration of NO achieved 11.5 ± 0.38 μM after 1 h and increased to 14.5 ± 0.4 μM after 12 h. In addition, the NO concentration remained stable at 14.5 ± 0.2 μM until 24 h. Due to the immobilization of Cu NPs on the coatings, Cu-Ch NPs exhibited the continuous catalytic release of NO within 24 h. A schematic of the NO release process is given in Fig. 5B. NO is a free radical with a short half-life (a few seconds), and after a while, NO loses the free radical state and returned to a stable state [15]. According to the NO release mechanism, the presence of copper is necessary for the catalytic process of NO release from the operating nitrite [15]. In the NO release mechanism from the structure of Cu-Ch NPs, copper element in the combination with nitrite could catalyze the production of NO from nitrite. In the conversion of copper (Cu^{+1}) to copper (Cu^{+2}), catalytic properties are performed to generate NO [15]. Therefore, in the NO producing system based on the Cu-Ch NPs, NO release was achieved by converting nitrite to NO in the presence of copper as a catalyst. The initial burst release of NO could be due to the high hydrophilicity of Cu-Ch-5 % [52]. The PBS quickly penetrated the polymer matrix and entered the nanoparticles into the solution. Our results were close to Fontana et al. [15] research, in which the initial NO release from the chitosan/copper/ cellulose complex was reported 15 ± 3.5 nmol/g. These results might be accompanied by hemocompatibility improvement, increased rate of EC proliferation, and increased rate of migration and coverage of the synthetic surface during both phases [53].

3.5. Protein adsorption

The protein adsorption on the surface of biomaterials is critical in determining the tissue-biomaterial interface. Proteins are denatured and transformed into a film on the metal surface, which inhibit corrosion in the bio-corrosion process [54]. The effects of Cu-Ch NP concentration (1, 3, and 5 wt%) on the protein adsorption was investigated (Fig. 6A). Before evaluation of BSA adsorption, the standard curve of BSA in the concentration range of 0.02–4(mg/ml) was provided (Fig. S2). The results showed a significant increase in the protein adsorption from 69.5 ± 0.7 μg/g to 522 ± 66.06 μg/g after the incorporation of 5 wt% Cu-Ch NPs ($P < 0.05$). This increase in protein adsorption was due to the presence of both copper and chitosan. According to recent studies, copper and chitosan are the agents that could enhance protein adsorption [55]. Thanks to the functional amine and hydroxyl groups in the chitosan structure, chitosan shows excellent BSA adsorption. Bumgardner et al. [56] significantly enhanced protein adsorption by applying chitosan coatings on titanium substrates. In this study, albumin protein absorption enriched from 0.4 μg/mm^2 to 0.55 μg/mm^2 with the formation of chitosan coating on bare titanium. Protein adsorption has a significant impact on the hemocompatibility. Increased protein adsorption may cause blood clotting and platelet adhesion. However, recent studies indicated that protein adsorption <1 mg/g might not disturb hemocompatibility [57].

3.6. Platelet adhesion

Platelet adhesion evaluation is the critical step to verify the hemocompatibility and biocompatibility of materials for cardiovascular applications. Depending on the surface properties of biomaterials, platelet adhesion is often the first reaction to the implant, which may stimulate blood coagulation and thrombosis [58]. Here, the platelet adhesion in contact with MAO/PGS/Cu-Ch NPs coatings was assessed. Due to the binding of plasma proteins on the surface of biological materials, platelets attached, aggregated, and formed thrombosis. SEM images of samples after platelet adhesion evaluation are provided in Fig. 6B. The round shape platelets were observed in our results which were similar to previous studies [59]. Results showed platelet adhesion reduced after the incorporation of Cu-Ch NPs in PGS coatings. Major et al. [60] also investigated platelet adhesion on polyurethane coatings by adding a NO production system containing Cu NPs. The results showed that the NO generating system could significantly reduce platelet adhesion. Furthermore, the presence of CuO in the coatings may also reduce the platelet adhesion. Ahmed et al. [61] also investigated platelet adhesion on chitosan-copper oxide nanocomposite coatings. The results showed that coatings containing chitosan and CuO significantly reduced platelet adhesion.

3.7. Endothelial cell culture

The role of Cu-Ch NPs on the toxicity of coatings was investigated using MTT assay after 1, 3, and 5 days of culture. Fig. 6C shows significantly improved cell survival in contact with bilayer coatings containing 1, 3, and 5 wt% Cu-Ch NPs compared to Cu-Ch-0 % during 5 days of culture. For example, after 5 days of culture, the cell viability significantly increased from 97 ± 2 (%control) in Cu-Ch-0 % to 110 ± 2 (% control) in Ch-Ch-5 % ($P < 0.05$). In addition, by increasing culture time from day 1 to day 5, cell viability enhanced in all samples confirming the cytocompatibility of samples. In addition, due to the viability of >90 % in all samples, it was obvious that the degradation byproducts and released copper element were not toxic to HUVECs. This non-toxicity of copper in polymer coatings was also found in recent studies. Trickler et al. [62] also demonstrated that Cu nanoparticle concentrations of >12.5 mg/l significantly impacted cellular behavior and remarkably

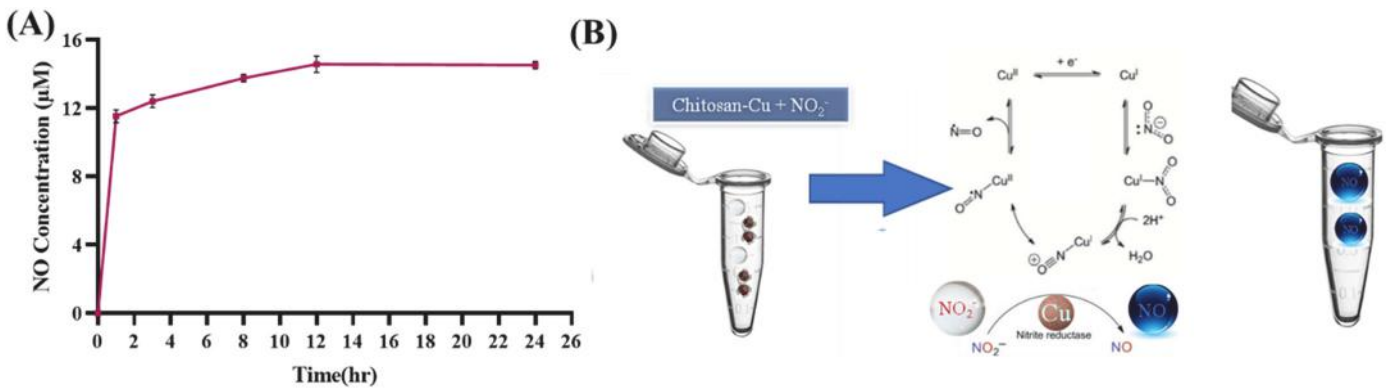

Fig. 5. (A) The NO release profile of Cu-Ch-5 % upon 24 h and (B) the schematic of the NO release process via catalytic properties of copper.

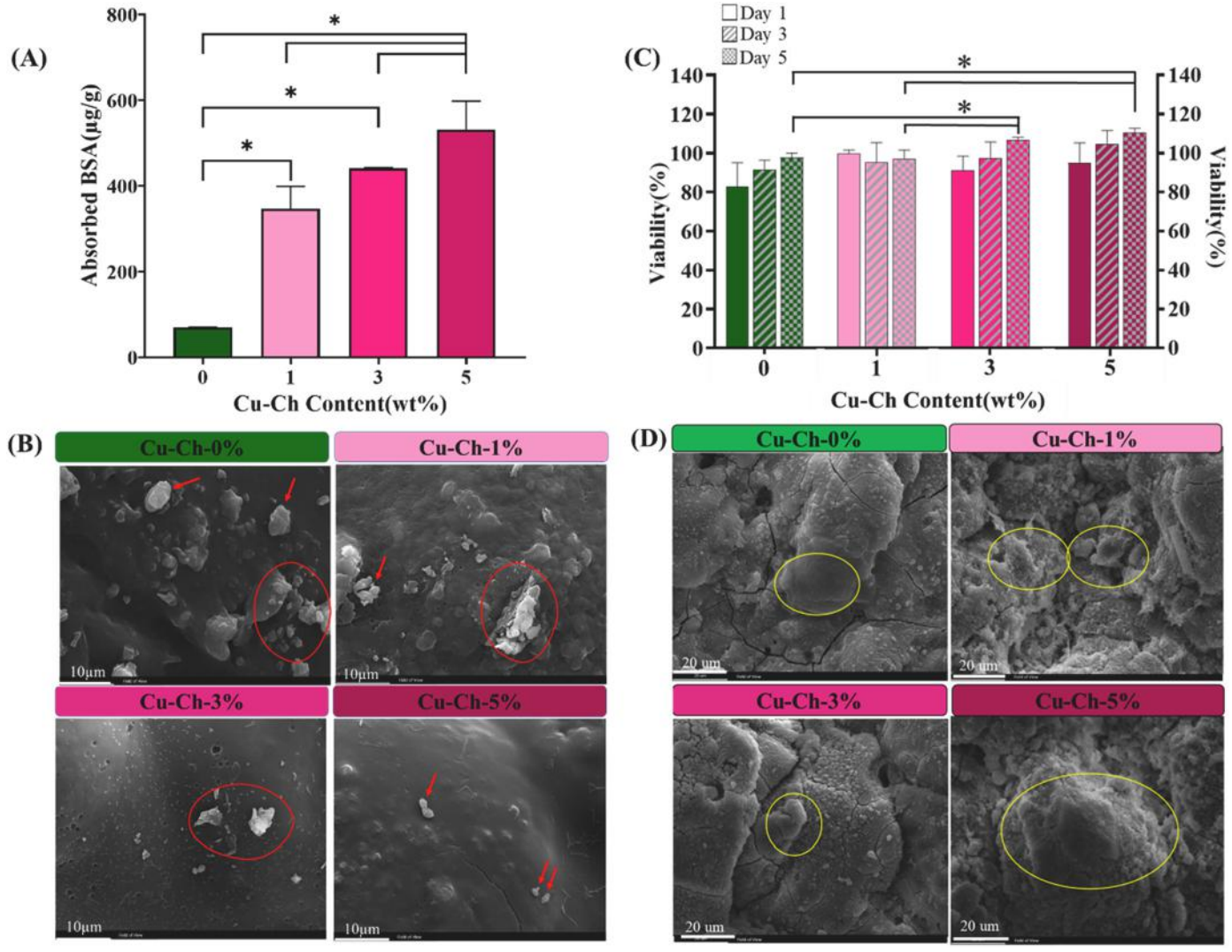

Fig. 6. The biological properties of MAO-PGS/Cu-Ch NPs coatings:(A) BSA Adsorption, (B) SEM images of platelet adhesion (platelets are marked with red arrows and circles), (C) the viability of HUVECs after 1, 3 and 5 days of incubation measured using MTT assay (D) SEM images of HUVECs seeded on the samples for three days (cells are marked with yellow circles) (*: significant difference, *: $P < 0.05$). (For interpretation of the references to color in this figure legend, the reader is referred to the web version of this article.).

reduced cellular proliferation. Moreover, our ICP results demonstrated that the concentration of copper ions released from Cu-Ch-1 %, Cu-Ch-3 % and Cu-Ch-5 % samples after 5 days incubation was determined 0.08 mg/l, 0.14 mg/l and 0.2 mg/l, respectively, which was less than the above critical concentration. According to recent studies, copper ions could increase the angiogenin binding to ECs and stimulate several intracellular events [63].

Cell adhesion and spreading are among the essential features to show the biocompatibility of the implant with the target tissue. The SEM images of HUVECs seeded coatings in Fig. 6D demonstrated the HUVECs attached and spread on the coatings (marked with yellow circles). In addition to the increase in the number of cells spread on the coatings, some cells could penetrate into the porous structures, over the culture time. Generally, the chemical composition of coatings has a crucial role in cell adhesion because any inhibitory and toxicity influence cell viability [38]. According to our results, HUVEC adhesion to the samples improved after the incorporation of Cu-Ch NPs, especially on the Cu-Ch-5 % sample indicating no toxicity and inhibitory composition. In addition, NO may have a dramatic impact on HUVECs adhesion and proliferation. According to our results, enhancement in HUVECs adhesion after Cu-Ch NPs interpolation was observed which might be related to the NO release aspect. Yang et al. [16] confirmed that the NO catalytic surface enhanced adhesion and proliferation of HUVECs on 3,3-diselenodipropionic acid (SeDPA) and SeDPA-plasma polymerized allylamine (SeDPA-PPAam) coatings. Fontana et al. [15] also discovered that combining the NO-releasing copper-chitosan system achieved a 130 % increase in ARPE-19 cell growth compared to other samples without copper NO catalyst. Another factor in cell adhesion is the surface morphology and roughness. Our results suggested that increasing surface roughness may also improve cell adhesion. Additionally, on coatings with high surface roughness, cells may attach and spread more effectively. Hallab et al. [64] investigated the effect of surface roughness of three polymers of polytetrafluoroethylene, high-density polyethylene, and plastic silicon on cellular behavior. They showed that with increasing surface roughness in the range of 1–10 μm, cell adhesion also significantly increased. In another study, Zhou et al. [38] investigated the effects of surface roughness on endothelial cell attachment on the magnesium alloy with a two-layer MgF/polydopamine coating for three days. In this study, with increasing surface roughness from 0.01 μm to 2 μm, the density of endothelial cells increased from 180 cells/mm^2 to 350 cells/mm^2. Our findings showed that coatings containing Cu-Ch NPs not only provided suitable corrosion resistance and NO-release catalytic

feature but could also encourage cell function, making it an excellent biocompatible substance for tissue engineering.

4. Conclusion

In summary, we developed a NO-release bilayer MAO-PGS coatings containing various Cu-Ch NP concentrations and studied their physicochemical properties, surface features, corrosion behavior, and biological properties. Functionalization of MAO-PGS surface with such NO-release catalytic Cu-Ch NPs enhanced some specific characteristics such as surface roughness, corrosion behavior, and protein adsorption, while the adhesion strength was not significantly changed. Bilayer MAO-PGS/Cu-Ch NPs coating provided NO release in two phases of burst release followed by extended-release leading to significant inhibitory effects on the platelet activation and adhesion. In addition, Cu-Ch NPs were not only nontoxic to HUVEC, but also encouraged cell viability, proliferation, and adhesion. In summary, this research may contain broad advantages for the design of vascular devices and stimulate the development of the upcoming generation of vascular stents.

CRediT authorship contribution statement

M. G.: Investigation, Writing the original work, Visualization, Formal analysis, Software.

M.K.: Supervision, Project administration, Funding acquisition, Conceptualization.

M.A.: Supervision, Funding acquisition, Conceptualization.

P.H.: Writing the original work, Formal analysis.

Declaration of competing interest

The authors have no affiliation with any organization with a direct or indirect financial interest in the subject matter discussed in the manuscript.

Data availability

Data will be made available on request.

Appendix A. Supplementary data

Supplementary data to this article can be found online at https://doi.org/10.1016/j.porgcoat.2022.107269.

References

[1] R. Rikhtegar, M. Pezeshkian, S. Dolati, N. Safaie, A.A. Rad, M. Mahdipour, M. Nouri, A.R. Jodati, M. Yousefi, Stem cells as therapy for heart disease: iPSCs, ESCs, CSCs, and skeletal myoblasts, Biomed. Pharmacother. 109 (2019) 304–313.

[2] N. Sezer, Z. Evis, S.M. Kayhan, A. Tahmasebifar, M. Koç, Review of magnesium-based biomaterials and their applications, J. Magnes. Alloys 6 (1) (2018) 23–43.

[3] Y.-J. Shi, J. Pei, J. Zhang, J.-L. Niu, H. Zhang, S.-R. Guo, Z.-H. Li, G.-Y. Yuan, Enhanced corrosion resistance and cytocompatibility of biodegradable Mg alloys by introduction of mg (OH) 2 particles into poly (L-lactic acid) coating, Sci. Rep. 7 (2017) 41796.

[4] S. Farshid, M. Kharaziha, Micro and nano-enabled approaches to improve the performance of plasma electrolytic oxidation coated magnesium alloys, J. Magnes. Alloys 9 (5) (2020) 1487–1504.

[5] L.V. Parfenova, Z.R. Galimshina, G.U. Gil'fanova, E.I. Alibaeva, K.V. Danilko, T. M. Pashkova, O.L. Kartashova, R.G. Farrakhov, V.R. Mukaeva, E.V. Parfenov, R. Nagumothu, R.Z. Valiev, Hyaluronic acid bisphosphonates as antifouling antimicrobial coatings for PEO-modified titanium implants, Surf. Interfaces 28 (2022), 101678.

[6] Z.-Z. Yin, W.-C. Qi, R.-C. Zeng, X.-B. Chen, C.-D. Gu, S.-K. Guan, Y.-F. Zheng, Advances in coatings on biodegradable magnesium alloys, J. Magnes. Alloys 8 (1) (2020) 42–65.

[7] A.G. Olaru, V. Butculescu, C. Dumitriu, N. Badea, S. Popescu, C. Ungureanu, C. Pirvu, Biopolymers as intermediate layers for amoxicillin grafting on antibacterial surface, Surf. Interfaces 33 (2022), 102224.

[8] W. Zhuang, G. Ye, J. Wu, L. Wang, G. Fang, Z. Ye, G. Lai, X. Qiu, H. Sang, A 3D-printed bioactive polycaprolactone scaffold assembled with core/shell microspheres as a sustained BMP2-releasing system for bone repair, Biomater. Adv. 133 (2022), 112619.

[9] M. Ghafarzadeh, M. Kharaziha, M. Atapour, Bilayer micro-arc oxidation-poly (glycerol sebacate) coating on AZ91 for improved corrosion resistance and biological activity, Prog. Org. Coat. 161 (2021), 106495.

[10] R. Rai, M. Tallawi, A. Grigore, A.R. Boccaccini, Synthesis, properties and biomedical applications of poly (glycerol sebacate)(PGS): a review, Prog. Polym. Sci. 37 (8) (2012) 1051–1078.

[11] Z. Wei, P. Tian, X. Liu, B. Zhou, Hemocompatibility and selective cell fate of polydopamine-assisted heparinized PEO/PLLA composite coating on biodegradable AZ31 alloy, Colloids Surf. B: Biointerfaces 121 (2014) 451–460.

[12] Y. Ikeda, S. Tajima, S. Yoshida, N. Yamano, Y. Kihira, K. Ishizawa, K. Aihara, S. Tomita, K. Tsuchiya, T. Tamaki, Deferoxamine promotes angiogenesis via the activation of vascular endothelial cell function, Atherosclerosis 215 (2) (2011) 339–347.

[13] F. Xie, L. Feng, W. Cai, Y. Qiu, Y. Liu, Y. Li, B. Du, L. Qiu, Vaccarin promotes endothelial cell proliferation in association with neovascularization in vitro and in vivo, Mol. Med. Rep. 12 (1) (2015) 1131–1136.

[14] C.-G. Wang, Y.-T. Lou, M.-J. Tong, L.-L. Zhang, Z.-J. Zhang, Y.-Z. Feng, S. Li, H.-Z. Xu, C. Mao, Asperosaponin VI promotes angiogenesis and accelerates wound healing in rats via up-regulating HIF-1α/VEGF signaling, Acta Pharmacol. Sin. 39 (3) (2018) 393–404.

[15] K. Fontana, L. Ventimiglia, B. Mutus, Nitric oxide generating copper–chitosan particles for wound healing applications, J. Chem. Technol. Biotechnol. 93 (8) (2018) 2093–2101.

[16] Z. Yang, Y. Yang, K. Xiong, X. Li, P. Qi, Q. Tu, F. Jing, Y. Weng, J. Wang, N. Huang, Nitric oxide producing coating mimicking endothelium function for multifunctional vascular stents, Biomaterials 63 (2015) 80–92.

[17] Y. Zhang, S. Cui, S. Cao, L. Yang, G. Qin, E. Zhang, To improve the angiogenesis of endothelial cells on ti-cu alloy by the synergistic effects of cu ions release and surface nanostructure, Surf. Coat. Technol. 433 (2022), 128116.

[18] E. Tabesh, H. Salimijazi, M. Kharaziha, M. Hejazi, Antibacterial chitosan-copper nanocomposite coatings for biomedical applications, Materials Today: Proceedings 5 (7, Part 3) (2018) 15806–15812.

[19] N. Rajabi, M. Kharaziha, R. Emadi, A. Zarrabi, H. Mokhtari, S. Salehi, An adhesive and injectable nanocomposite hydrogel of thiolated gelatin/gelatin methacrylate/Laponite® as a potential surgical sealant, J. Colloid Interface Sci. 564 (2020) 155–169.

[20] M. Akgül, N.B. Savak, M. Özmak, A.G. Dumanli, Y. Yürüm, A. Karabakan, Adsorption of bovine serum albumin BSA on Clinoptilolite, Hacettepe Journal of Biology and Chemistry 36 (1) (2008) 21–29.

[21] H. Mokhtari, Z. Ghasemi, M. Kharaziha, F. Karimzadeh, F. Alihosseini, Chitosan-58S bioactive glass nanocomposite coatings on TiO2 nanotube: structural and biological properties, Appl. Surf. Sci. 441 (2018) 138–149.

[22] A. Talebi, S. Labbaf, M. Atari, M. Parhizkar, Polymeric nanocomposite structures based on functionalized graphene with tunable properties for nervous tissue replacement, ACS Biomater. Sci. Eng. 7 (9) (2021) 4591–4601.

[23] K.G. Mann, M.F. Whelihan, S. Butenas, T. Orfeo, Citrate anticoagulation and the dynamics of thrombin generation, J. Thromb. Haemost. 5 (10) (2007) 2055–2061.

[24] T. Jayaramudu, K. Varaprasad, R.D. Pyarasani, K.K. Reddy, K.D. Kumar, A. Akbari-Fakhrabadi, R. Mangalaraja, J. Amalraj, Chitosan capped copper oxide/copper nanoparticles encapsulated microbial resistant nanocomposite films, Int. J. Biol. Macromol. 128 (2019) 499–508.

[25] P.K. Raul, S. Senapati, A.K. Sahoo, I.M. Umlong, R.R. Devi, A.J. Thakur, V. Veer, CuO nanorods: a potential and efficient adsorbent in water purification, RSC Adv. 4 (76) (2014) 40580–40587.

[26] X. Zhou, D. Liu, H. Bu, L. Deng, H. Liu, P. Yuan, P. Du, H. Song, XRD-based quantitative analysis of clay minerals using reference intensity ratios, mineral intensity factors, Rietveld, and full pattern summation methods: a critical review, Solid Earth Sciences 3 (1) (2018) 16–29.

[27] M. Fernandes Queiroz, K.R.T. Melo, D.A. Sabry, G.L. Sassaki, H.A.O. Rocha, Does the use of chitosan contribute to oxalate kidney stone formation? Mar. Drugs 13 (1) (2015) 141–158.

[28] M.S. Usman, M.E. El Zowalaty, K. Shameli, N. Zainuddin, M. Salama, N.A. Ibrahim, Synthesis, characterization, and antimicrobial properties of copper nanoparticles, Int. J. Nanomedicine 8 (2013) 4467.

[29] U. Sakulkhu, M. Mahmoudi, L. Maurizi, G. Coullerez, M. Hofmann-Amtenbrink, M. Vries, M. Motazacker, F. Rezaee, H. Hofmann, Significance of surface charge and shell material of superparamagnetic iron oxide nanoparticle (SPION) based core/shell nanoparticles on the composition of the protein corona, Biomater. Sci. 3 (2) (2015) 265–278.

[30] M.S.S.A. Saraswathi, D. Rana, K. Divya, S. Gowrishankar, A. Nagendran, Versatility of hydrophilic and antifouling PVDF ultrafiltration membranes tailored with polyhexanide coated copper oxide nanoparticles, Polym. Test. 84 (2020), 106367.

[31] D. Narayan, S. Venkatraman, Effect of pore size and interpore distance on endothelial cell growth on polymers, J. Biomed. Mater. Res. A 87 (3) (2008) 710–718.

[32] M. Park, J.E. Lee, C.G. Park, S.H. Lee, H.K. Seok, Y.B. Choy, Polycaprolactone coating with varying thicknesses for controlled corrosion of magnesium, J. Coat. Technol. Res. 10 (5) (2013) 695–706.

[33] A. Vijayan, SA, G.S.V. Kumar, PEG grafted chitosan scaffold for dual growth factor delivery for enhanced wound healing, Scientific Reports 9 (1) (2019) 19165.

[34] M. Alaei, M. Atapour, S. Labbaf, Electrophoretic deposition of chitosan-bioactive glass nanocomposite coatings on AZ91 Mg alloy for biomedical applications, Prog. Org. Coat. 147 (2020), 105803.

[35] M.M. Ouberai, K. Xu, M.E. Welland, Effect of the interplay between protein and surface on the properties of adsorbed protein layers, Biomaterials 35 (24) (2014) 6157–6163.
[36] J. Lu, C. Yao, L. Yang, T.J. Webster, Decreased platelet adhesion and enhanced endothelial cell functions on nano and submicron-rough titanium stents, Tissue Eng. A 18 (13–14) (2012) 1389–1398.
[37] E. Mahlooji, M. Atapour, S. Labbaf, Electrophoretic deposition of bioactive glass – chitosan nanocomposite coatings on ti-6Al-4V for orthopedic applications, Carbohydr. Polym. 226 (2019), 115299.
[38] K. Zhou, Y. Li, L. Zhang, L. Jin, F. Yuan, J. Tan, G. Yuan, J. Pei, Nano-micrometer surface roughness gradients reveal topographical influences on differentiating responses of vascular cells on biodegradable magnesium, Bioact. Mater. 6 (1) (2021) 262–272.
[39] F. Ahmadi, Z. Oveisi, S.M. Samani, Z. Amoozgar, Chitosan based hydrogels: characteristics and pharmaceutical applications, Res. Pharm. Sci. 10 (1) (2015) 1–16.
[40] M. Fadaie, E. Mirzaei, B. Geramizadeh, Z. Asvar, Incorporation of nanofibrillated chitosan into electrospun PCL nanofibers makes scaffolds with enhanced mechanical and biological properties, Carbohydr. Polym. 199 (2018) 628–640.
[41] S. Kakinoki, S. Nishioka, Y. Arichi, T. Yamaoka, Stable and direct coating of fibronectin-derived leu-asp-val peptide on ePTFE using one-pot tyrosine oxidation for endothelial cell adhesion, Colloids Surf. B: Biointerfaces 216 (2022), 112576.
[42] J. Dong, M. Pacella, Y. Liu, L. Zhao, Surface engineering and the application of laser-based processes to stents-a review of the latest development, Bioact. Mater. 10 (2022) 159–184.
[43] A.J. Nathanael, T.H. Oh, Biopolymer coatings for biomedical applications, Polymers 12 (12) (2020) 3061.
[44] S. Budhe, A. Ghumatkar, N. Birajdar, M. Banea, Effect of surface roughness using different adherend materials on the adhesive bond strength, Appl. Adhes. Sci. 3 (1) (2015) 1–10.
[45] E. Dayss, G. Leps, J. Meinhardt, Surface modification for improved adhesion of a polymer–metal compound, Surf. Coat. Technol. 116–119 (1999) 986–990.
[46] A. Necati, The effect of cu nanoparticle adding on to epoxy-based adhesive and adhesion properties, Sci. Rep. 10 (1) (2020) 11038.
[47] S. Panin, D. Nguyen, L. Kornienko, D. Buslovich, M. Lerner, Mechanical and tribological properties of thermoplastic polyetheretherketone based nanocomposites, in: AIP Conference Proceedings, AIP Publishing LLC, 2020, p. 040006.
[48] E. Tabesh, H.R. Salimijazi, M. Kharaziha, M. Mahmoudi, M. Hejazi, Development of an in-situ chitosan-copper nanoparticle coating by electrophoretic deposition, Surf. Coat. Technol. 364 (2019) 239–247.
[49] H. Ashassi-Sorkhabi, A. Kazempour, Chitosan, its derivatives and composites with superior potentials for the corrosion protection of steel alloys: a comprehensive review, Carbohydr. Polym. 237 (2020), 116110.
[50] I. Kozina, H. Krawiec, M. Starowicz, M. Kawalec, Corrosion resistance of MgZn alloy covered by chitosan-based coatings, Int. J. Mol. Sci. 22 (15) (2021) 8301.
[51] H.A. El Shayeb, E.N. El Sawy, Corrosion behaviour of pure mg, AS31 and AZ91 in buffered and unbuffered sulphate and chloride solutions, Corros. Eng. Sci. Technol. 46 (4) (2011) 481–492.
[52] X. Huang, C.S. Brazel, On the importance and mechanisms of burst release in matrix-controlled drug delivery systems, J. Control. Release 73 (2–3) (2001) 121–136.
[53] J. Rao, H. Pan Bei, Y. Yang, Y. Liu, H. Lin, X. Zhao, Nitric oxide-producing cardiovascular stent coatings for prevention of thrombosis and restenosis, Front. Bioengi. Biotechnol. 8 (2020) 578.
[54] M. Talha, Y. Ma, P. Kumar, Y. Lin, A. Singh, Role of protein adsorption in the bio corrosion of metallic implants–a review, Colloids Surf. B: Biointerfaces 176 (2019) 494–506.
[55] G. Li, J. Huang, T. Chen, X. Wang, H. Zhang, Q. Chen, Insight into the interaction between chitosan and bovine serum albumin, Carbohydr. Polym. 176 (2017) 75–82.
[56] J.D. Bumgardner, R. Wiser, S.H. Elder, R. Jouett, Y. Yang, J.L. Ong, Contact angle, protein adsorption and osteoblast precursor cell attachment to chitosan coatings bonded to titanium, J. Biomater. Sci Polym. Ed. 14 (12) (2003) 1401–1409.
[57] N. Golafshan, R. Rezahasani, M.T. Esfahani, M. Kharaziha, S. Khorasani, Nanohybrid hydrogels of laponite: PVA-alginate as a potential wound healing material, Carbohydr. Polym. 176 (2017) 392–401.
[58] L.B. Koh, I. Rodriguez, S.S. Venkatraman, The effect of topography of polymer surfaces on platelet adhesion, Biomaterials 31 (7) (2010) 1533–1545.
[59] A.-L. Papa, A. Jiang, N. Korin, M.B. Chen, E.T. Langan, A. Waterhouse, E. Nash, J. Caroff, A. Graveline, A. Vernet, Platelet decoys inhibit thrombosis and prevent metastatic tumor formation in preclinical models, Sci. Transl. Med. 11 (479) (2019) eaau5898.
[60] T.C. Major, D.O. Brant, C.P. Burney, K.A. Amoako, G.M. Annich, M.E. Meyerhoff, H. Handa, R.H. Bartlett, The hemocompatibility of a nitric oxide generating polymer that catalyzes S-nitrosothiol decomposition in an extracorporeal circulation model, Biomaterials 32 (26) (2011) 5957–5969.
[61] S.B. Ahmed, H.I. Mohamed, A.M. Al-Subaie, A.I. Al-Ohali, N.M.R. Mahmoud, Investigation of the antimicrobial activity and hematological pattern of nano-chitosan and its nano-copper composite, Sci. Rep. 11 (1) (2021) 9540.
[62] W.J. Trickler, S.M. Lantz, A.M. Schrand, B.L. Robinson, G.D. Newport, J. J. Schlager, M.G. Paule, W. Slikker, A.S. Biris, S.M. Hussain, Effects of copper nanoparticles on rat cerebral microvessel endothelial cells, Nanomedicine 7 (6) (2012) 835–846.
[63] J. Salvo, C. Sandoval, Role of copper nanoparticles in wound healing for chronic wounds: literature review, Burns Trauma 10 (2022).
[64] N.J. Hallab, K.J. Bundy, K. O'Connor, R.L. Moses, J.J. Jacobs, Evaluation of metallic and polymeric biomaterial surface energy and surface roughness characteristics for directed cell adhesion, Tissue Eng. 7 (1) (2001) 55–71.